Journal for
Electrochemistry and
Plating Technology

JEPT

Edited by: DGO-Fachausschuss Forschung – Hilden / Germany

Electrochemical Deposition and Microstructure Characterization of Lead-Tin-Layers

The present study investigated the formation of a binary alloy of lead and tin. Both elements represent a thermodynamic system with strongly limited miscibility in solid state. The deposition of the layers was carried out under potentiostatic conditions at various deposition potentials from a sulfonate-based electrolyte. The layer formation was characterized by electrochemical techniques (cyclovoltammetry, chronoamperometry). The microstructure development was investigated by SEM/EDX measurements and X-ray diffraction. The layer formation is compliant with the Stranski-Krastanov growth mode. The current efficiency of the deposition was approximately 100%. According to the thermodynamic theory the layers show a dual-phase microstructure. The composition of the Pb-Sn layers was depending on the deposition potential. Supersaturated α-Pb-solid...

Received: 2012-08-16
Received in revised form: 2012-10-03
Accepted: 2012-11-15

Keywords: electrolytic deposition, microstructure, Pb-Sn alloys, deposition kinetic

By M. Schneider, K. Kremmer, B. Matthey

LEUZE VERLAG
seit 1902

Electrochemical Deposition and Microstructure Characterization of Lead-Tin-Layers

M. Schneider[1], K. Kremmer[1], B. Matthey[1]
Corresponding author: M. Schneider, E-Mail: michael.schneider@ikts.fraunhofer.de
1 Fraunhofer Institute for Ceramic Technologies and Systems Dresden, Winterbergstr. 27, 01277 Dresden, Germany

The present study investigated the formation of a binary alloy of lead and tin. Both elements represent a thermodynamic system with strongly limited miscibility in solid state. The deposition of the layers was carried out under potentiostatic conditions at various deposition potentials from a sulfonate-based electrolyte. The layer formation was characterized by electrochemical techniques (cyclovoltammetry, chronoamperometry). The microstructure development was investigated by SEM/EDX measurements and X-ray diffraction. The layer formation is compliant with the Stranski-Krastanov growth mode. The current efficiency of the deposition was approximately 100%. According to the thermodynamic theory the layers show a dual-phase microstructure. The composition of the Pb-Sn layers was depending on the deposition potential. Supersaturated α-Pb-solid solution could not be observed. The morphology is also strongly depending on the deposition potential. The diffusion coefficient of the metal ions in the sulfonat-based electrolyte was measured by rotating disc electrode experiments. The formal diffusion coefficient in the electrolyte containing Pb^{2+}- and Sn^{2+}- ions is close to the diffusion coefficient of lead ions.

Keywords: electrolytic deposition, microstructure, Pb-Sn alloys, deposition kinetic
Paper: Received: 2012-08-16 / Received in revised form: 2012-10-03 / Accepted: 2012-11-15

1 Introduction

The electrochemical deposition (ECD) of lead, tin and their alloys are part of the oldest processes in electroplating [1]. Extraordinary relevance achieved tin-lead alloys (e.g. 90%Sn/10%Pb) as soldering material, but also lead-tin alloys (e.g.93%Pb/7%Sn) as corrosion protective coatings on steel ("Terne plate") or bearing metal (e.g. 95%Pb/5%Sn) [2–8]. Lead (fcc) and tin (hcp) forms an eutectic binary system with strongly limited solubility of tin in lead (<1mass-%) at room temperature. The solubility of lead in tin is negligible at room temperature [3].

Regarding the electrolytic deposition the system Pb-Sn it is interesting, on the one hand to study the formation of a polyphase alloy (α-Pb and β-Sn). On the other hand, lead-tin alloys can be easily deposited because the standard potential of both elements differs only by 10mV. Additionally, the hydrogen over voltage η_{H_2} on both metals is relatively high (Pb electroplated: $\eta_{H_2} = 0.91V$ at 1mAcm^{-2}; Sn: $\eta_{H_2} = 0.85V$ at 1mAcm^{-2} [9]). Therefore, also in acidic electrolyte the deposition can take place without co-deposition of hydrogen. Typical electrolytes are acidic fluoroborate or sulfonate based electrolytes, whereby the sulfonat-based electrolyte is less toxic [2] and was

preferred in this work. In the industrial process the composition of the deposited alloy can easily be controlled by the relation of the ion concentration of the elements in the plating bath. Additionally, commercial plating bath contains additional additives to achieve fine-grained and shiny coatings [2]. As *Palmisano et al.* reported, additives influence the kinetic of the deposition process. They observed diffusion-controlled lead deposition in the absence of the additive, whereas the process is charge-transfer controlled in the presence of the additive [10]. Petersson et al. [11, 12] investigated the electrodeposition of Pb-Sn alloys in additive free fluoroborate based electrolyte. Their work was focused on the deposition kinetic within a potential range between $-430mV_{Ag/AgCl}$ and $-520mV_{Ag/AgCl}$ and the variation of concentration ratio between Pb- and Sn-ions. They found a 3D growing mechanism independent of the used substrate material [11, 12].

The intention of the present work was the investigation of the interplay between the applied deposition potential and the electrolytic formation of Pb-Sn layers. The selected electrolyte (sulphonate-based) should be of commercial interest and should have a lower toxicity in comparison with the well-known fluoroborate-based electrolyte.

In the focus of our interest were the following issues:

- the determination of the kinetic of the deposition and the rate-determining process,
- the investigation of the chemical composition of the deposited Pb-Sn layer depending on the deposition potential, and
- the development of the microstructure depending on the deposition potential.

Based on the aforementioned literature, we have abstained of additives in order to avoid any influence of the overvoltage of the deposition.

2 Experimental

2.1 Electrochemical deposition and investigation

The electrochemical deposition of Pb-Sn layers was realized in an aerated electrolyte consisting of methane sulphonic acid, lead sulphonate and tin sulphonate (electrolyte C) at room temperature. For comparison only selected measurements were carried out in lead-free, (electrolyte B) respectively tin-free (electrolyte A) electrolytes. The exact compositions and pH-values are shown in *Table 1*.

All electrochemical measurements were carried out in a 3-electrode cell with a gold wire as the counter electrode and a saturated silver electrode (SSE) as the reference electrode. An evaporated gold onto a glass sample was used as a working electrode and substrate for the deposition. Only the cyclo voltammetric and the rotating disc electrode (RDE) measurements were used in a solid gold sample as a working electrode.

Tab. 1: Electrolyte composition

Electrolyte	CH_4O_3S / mol/l	$Pb(CH_3SO_3)_2$ / mol/l	$Sn(CH_3SO_3)_2$ / mol/l	pH-value
A	0.5	0.05		0
B	0.5		0.05	0
C	0.5	0.05	0.05	0

The RDE measurements were carried out with a platinized titanium expanded metal as the counter electrode. All potentials are given versus the saturated silver electrode (Ag/AgCl-sat.KCl E=–0.197V_{SHE}). The electrolyte was not stirred during the experiments. The cell was coupled with a computer controlled potentiostate PGU20 (*IPS Peter Schrems*). After the deposition the samples were rinsed with deionized water and dried.

2.2 X-ray diffraction and scanning electron microscopy

The microstructure (phase analysis, surface morphology and chemical composition) of the deposited Pb-Sn-layer was investigated by using X-ray diffraction (XRD) and scanning electron microscopy (SEM). The XRD-experiments were carried out on a XRD 3003 T/T diffractometer (*GE Inspection & Sensing Technologies*) using symmetric diffraction geometry, CuKα (40KV; 30mA) and a scintillation detector. A *Goebel*-mirror and a 0.5 mm slit are located in the primary beam and a 0.2 mm detector slit is located in the diffracted beam.

The surface morphology and the chemical composition were investigated by using a field-emission scanning electron microscope Gemini 982 and Ultra55 (*Carl Zeiss SMT AG*) coupled with an EDX-Analyzer INCA (*Oxdord Instrument GmbH)*.

3 Results and Discussion

3.1 Electrochemistry

Figure 1a shows the cyclovoltammogram on gold in the electrolyte A. According to equation <1>, the standard potential E^0 and the lead ion concentration of the electrolyte (0.05 mol/l) the equilibrium potential amounts to $E_{Pb^{2+}/Pb}$=*–384 mV*$_{SSE}$. Ongoing with the cathodic sweep the observed deposition of Pb starts at E=–450 mV and reaches a maximum of E=–520 mV (a). At more negative potentials the deposition is diffusion controlled. The Pb deposition proceeds as well after the potential reversal during the anodic sweep for short time. In the anodic sweep the current peak (b) at approximately *E=–320mV* represents the oxidation and dissolution of Pb according to equation <1>.

$$Pb^{2+}+2e^- \leftrightarrow Pb\ ;\quad E^0=-0.126V_{SHE} \qquad <1>$$

At the end of the anodic sweep the Pb layer is completely dissolved and removed from the gold surface. Both were observed

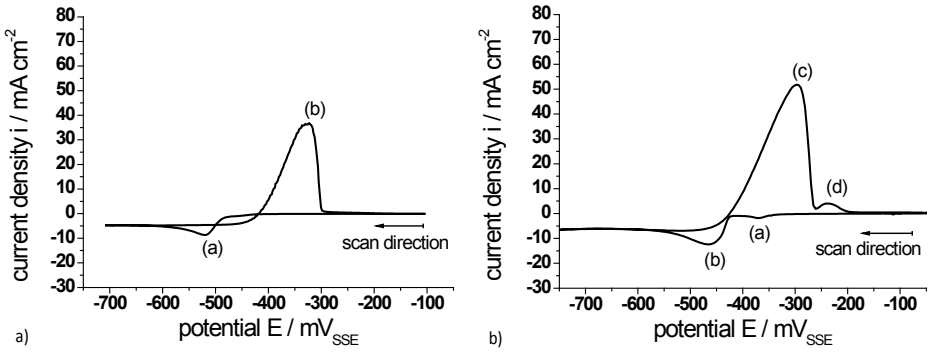

Fig. 1: Cyclovoltammogram (dE/dt=10mV/s) on Au in 10mV/s 0.5mol/l CH_4O_3S containing a) 0.05mol/l $Pb(CH_3SO_3)_2$ (electrolyte A) and b) 0.05mol/l $Sn(CH_3SO_3)_2$ (electrolyte B)

to have a current crossover on the anodic scan and is ascribed to a typical nucleation behavior, as reported by *Peterson et al.* [11].

Figure 1b shows the cyclovoltammogram on gold in electrolyte B. According to equation <2>, the standard potential E^0 [13] and the tin ion concentration of the electrolyte (0.05mol/l) the equilibrium potential amounts to $E_{Sn2+/Sn}$=–394mV$_{SSE}$.

$$Sn^{2+}+2e^- \leftrightarrow Sn \; ; \quad E^0=-0.136V_{SHE} \qquad <2>$$

However, the cyclic voltammogram shows four peaks. Thereby, the peak couple (b) and (c) represents the deposition and anodic dissolution of Sn, according to equation <2>. The weakly pronounced peak (a) can be explained by an under potential deposition (upd) of tin on gold as reported in the literature [12, 14]. The upd is associated with the incorporation of tin in the near surface range of gold [12]. The oxidation peak (d) can be explained by a secondary oxidation of Sn^{2+} to Sn^{4+} or SnO_2 according to equations <3a> and <3b>:

$$Sn^{2+} \rightarrow Sn^{4+}+2e^- \qquad <3a>$$

$$SN^{2+}+2H_2O \rightarrow SnO_2+4H^++2e^- \qquad <3b>$$

After cyclovoltammetry, a thin grey film remained on the surface to suggest the assumption of a consecutive reaction correspondent to equation <3b>.

Figure 2 shows the cyclovoltammogram on gold in electrolyte C. It can be regarded as a superposition of the cyclic voltammograms measured in electrolyte A and B. Except for peak (d) all peaks discussed on the basis of *Figure 1* are shown again in *Figure 2*. The over-potential deposition (opd) of Pb and Sn take place virtually in the same potential range. The overlapping of peaks could be expected, due to the small difference in the standard potentials of Pb and Sn and the equal concentration of ions. Thereby, the opd starts with the deposition of Pb caused by the slightly more positive standard potential. This hypothesis will be discussed later on the basis of the microstructure investigations. In comparison with the Pb deposition in *Figure 1a* it is evident that the decreasing overvoltage of the Pb deposition is caused by the upd of Sn on gold. The maximum of the opd current density and the diffusion-limited current density are approximately a summation of the corresponding current densities in

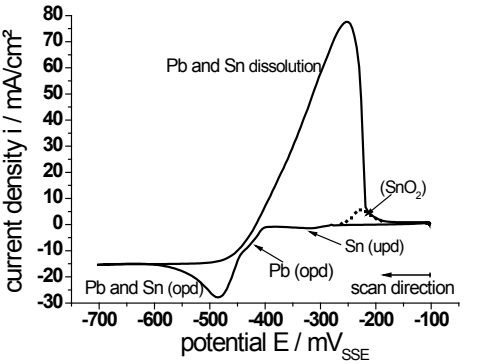

Fig. 2: Cyclovoltammogram (dE/dt=10mV/s) on Au in 10mV/s 0.5mol/l CH_4O_3S containing 0.05mol/l $Pb(CH_3SO_3)_2$ and 0.5mol/l $Sn(CH_3SO_3)_2$ (electrolyte C)

Figures 1a,b caused by the doubling of ion concentration in comparison to electrolytes A and B.

In view of the missing peak (d) from *Figure 1b* it should be assumed that the peak which represents the oxidation, according to equation 3b, is overlapped by the Pb- and Sn-dissolution peak. This is suggested by the dotted line in *Figure 2*. It should be noted that the dotted line is hand-drawn by the authors, based on the discussion

of *Figure 1b*. At the end of the experiment a thin grey film, presumably SnO_2, remains on the gold surface.

Based on these results, the PbSn-deposition was carried out at different applied potentials between E=–430mV and E=–660mV. *Figure 3* codifies to the thermodynamic point of view. At the most positive potential the deposition took place close to the equilibrium of Sn^{2+}/Sn as well as Pb^{2+}/Pb. It should be noted that the equilibrium potentials in the chosen electrolyte have slightly decreased as a result of the ion concentration of Pb and Sn in the solution.

Figure 4a shows the current transients during the potentiostatic deposition. Generally, after the modulation of the deposition potential the absolute value current density decreases rapidly to a steady-state with the exception of the current time transients at E=–630mV und E=–650mV. Since the deposition was charge-controlled, the deposition time varies depending on the current density. The defined charge limit in all experiments was Q_{limit}=1.056C. According to Faradays law and assuming a current efficiency κ=100%, the charge of Q_{limit}=1.056C corresponds to an intended thickness d_{Pb}=*2µm* for a pure Pb-layer.

The stationary current densities at a deposition time of t=120s are plotted in *Figure 4b*. Only the current densities at E=–630mV and E=–660mV are not stationary and increase continuously. The deposition can be distinguished into three regions (shown as Roman numerals I–III). Following the literature the deposition is initially activation controlled. At a higher over- voltage the influence of the diffusion increases continuously and the deposition is mixed- controlled [15]. The region (II) is characterized by the limited current density which is independent of the applied potential. In region (III) the current density rises again. Nev-

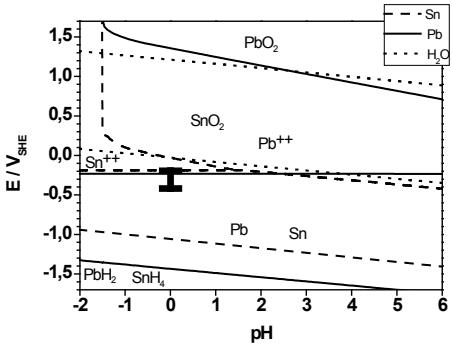

Fig. 3: Pourbaix-diagram of the system Pb-H_2O and Sn-H_2O in the pH range –2 to 6. The I represents the potential range of deposition between –430mV_{SSE} and –660mV_{SSE} which corresponds to –233mV_{SHE} and –463mV_{SHE} in the diagram above.

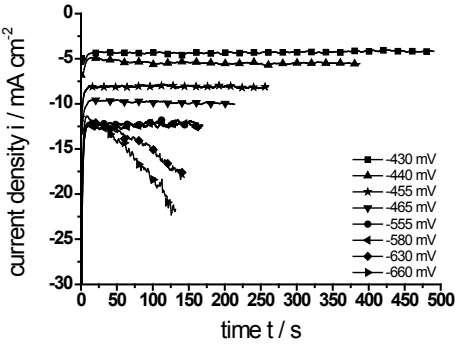

Fig. 4a: Current density versus deposition time (electrolyte C)

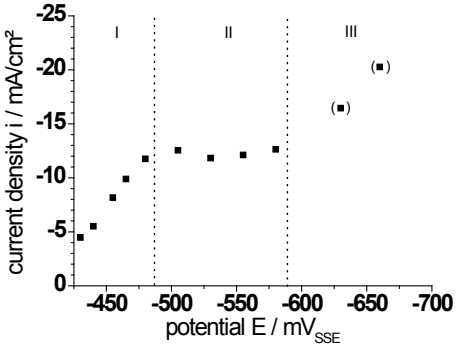

Fig. 4b: Steady state current density at t=120s extracted from Fig. 4a. The points in brackets are not steady state as shown in Fig. 4a.

ertheless, the kinetic is only diffusion controlled but the active surface increases as will be shown later. A current rise caused by the hydrogen evolution as a side reaction can be neglected because the necessary over-voltage η of this reaction (at 1mAcm^{-2}) amounts to η=0.95V for Pb and η=0.85V for Sn. Such a high voltage was never reached in our experiments. Additionally, this is in agreement with the cyclovoltammetric measurements (*Figs. 1, 2*) where no indication for hydrogen evolution can be observed.

Depending on the deposition potential the diffusion of Pb and Sn ion in the electrolyte plays a key role in view of the layer growth rate and the chemical composition. The usage of a rotating disc electrode (RDE) allows the investigation of the deposition, depending on the diffusion layer thickness, which can be positively adjusted by the rotating speed ω of the disc. In the case of a diffusion-only limited current density, the current depends on the ion concentration c_0 and the diffusion coefficient *D* and increases linearly with the square root of ω. These relations are described by *Levich*-equation (equation <4>):

$$i_{limit} = 0.62zFD^{\frac{2}{3}}\nu^{-\frac{1}{6}}c_o\omega^{\frac{1}{2}} \quad <4>$$

Whereby F represents the Faraday-constant, ν the viscosity of the electrolyte and z is the number of electrons. *Figure 5* shows the so called *Levich*-plot of i_{limit} versus the square root ω of the rotating disc.

Based on the data shown in *Figure 5* the diffusion coefficient can be calculated by rearrangement of equation <4> as follows:

$$D = \frac{2}{3}\sqrt{\frac{i_{limit}}{0.62zFc_0\nu^{-\frac{1}{6}}\omega^{\frac{1}{2}}}} \quad <4a>$$

The calculated diffusion coefficients according to equation <4a> are $D_{Pb}=8.5\cdot10^{-6}$ cm^2s^{-1} for Pb^{2+} (electrolyte A) and $D_{Sn}=4.4\cdot10^{-6}$ cm^2s^{-1} for Sn^{2+} (electrolyte B) under the chosen electrolyte conditions. The literature reports a diffusion coefficient $D=6.1\cdot10^{-6}$ – $9.7\cdot10^{-6}cm^2s^{-1}$ for Pb^{2+} under similar conditions [10, 12, 22], and for Sn^{2+} a diffusion coefficient $D=3\cdot10^{-6}$ – $6\cdot10^{-6}cm^2s^{-1}$ [23, 30].

The measured limited current density i_{limit} is the highest in electrolyte C caused by the twofold concentration c_0 of metal ions ($c_0^{(Pb2+)}$+ $c_0^{(Sn2+)}$). Based on the procedure described above the authors calculated a formal diffusion coefficient

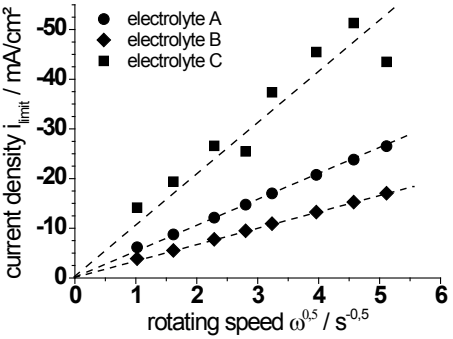

Fig. 5: Levich-plot of the diffusion limited current density at E=–550mV

$D_{form}=9.6\cdot10^{-6}cm^2s^{-1}$. That means the formal diffusion coefficient D_{form} is closer to D_{Pb} than to D_{Sn}. In this case the authors would expect a preferred deposition of Pb in the diffusion limited potential range. This is not the case as we show by EDX-analysis in section 3.2. Consequently, the diffusion of Pb- and Sn-ions in electrolyte C is not independent of each other.

3.2 Material characterization

Morphology

Figure 6 shows the surface morphology of PbSn-layer deposited at three different potentials which are representative for the regions I–III in *Figure 4*. The development of the morphology from region I to region III is comparable to the proposed growth types introduced by Fischer [9, 16] and later simplified by Winand [17]. These authors allocated the formation of specific growth types with two parameters, the inhibition intensity and the relation of i/c_{Me+} or i/i_{limit}, whereby the inhibition intensity is not quantitatively described. At low overvoltage (region I) the morphology appears compact and is mainly of the basis-orientated reproduction type.

In region II and III (*Figs. 6b, c*) the field orientated isolated crystal type are dominant. Thereby, in region II the relation $i/i_{limit} \cong 1$ and the morphology are characterized by isolated columnar crystallites. Again, in region II were the relation $i/i_{limit} > 1$ the morphology is decidedly dendritic or spongy. In agreement with the literature [9–17] the appearance of isolated columnar crystallites and dendrites is a sign of low inhibition intensity. The morphology development shown is associated with an extremely increased surface in region III which is compatible with the results shown in *Figure 4*. *Figure 7* shows a larger magnification of surface morphology of two samples formed at E=–440mV and E=–465mV. Both potentials are within the described region I of *Figure 4*. As aforementioned, this region is characterized by compact layers. However, the crystallite size d_k is apparently reciprocal in proportion to the overvoltage and to the current density, respectively (*Figs. 7a, c*).
This is well known (see e.g. [20]) and can be explained by the relation i/c_{Me+} because the decreasing concentration of metal ions inhibits the nucleus growth. *Figures 7b, d* shows backscatter images (atomic number contrast) of the sample sites shown in *Figures 7b, c*. The brighter

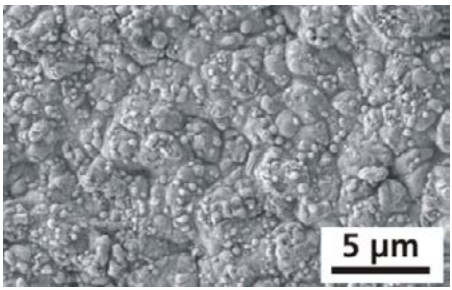

a) E=–430mV$_{SSE}$, SE-image

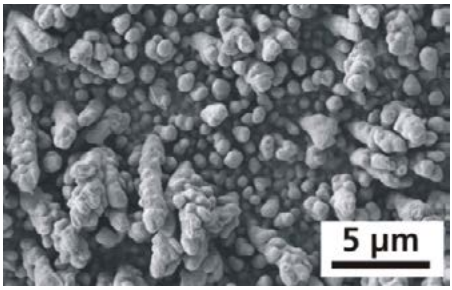

b) E=–555mV$_{SSE}$, SE-image

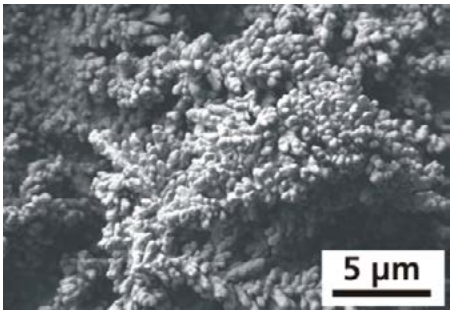

c) E=–660mV$_{SSE}$, SE-image

Fig. 6. SEM-images of the Pb-Sn layer morphology formed during the deposition in the described region I (a), II (b) and III (c)

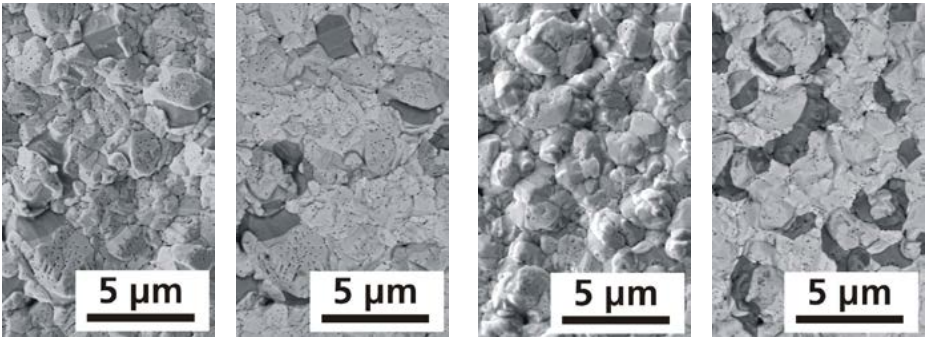

a) ECD at E=–440mV$_{SSE}$, SE-image

b) ECD at E=–440mV$_{SSE}$, BSE-image

c) ECD at E=–465mV$_{SSE}$, SE-image

d) ECD at E=–465mV$_{SSE}$, BSE-image

Fig. 7: SEM-images of the morphology of Pb-Sn layer formed at various deposition potentials in the described region I from Fig. 4.

area is the Pb phase (higher atomic number) the darker area is the β-Sn phase (lower atomic number). It should be noted that the higher the overvoltage the higher the part of β-Sn. Both, Pb and Sn are separately deposited as expected from the thermodynamic point of view (*see later on in Fig. 9*) [19]. A high number of very small pores are visible. The reason of the pores is not absolutely clear but also visible in the images published by *Peterson et al.* [12].

EDX-analysis and chemical composition

Figure 8 shows the results of EDX-measurements calculated as an atomic percentage of lead and tin. It is evident that at a very low overvoltage the content of Pb dominates the layer composition. This can be explained by the slightly more positive equilibrium potential $E_{Pb/Pb^2} = -384mV_{SSE}$ in comparison to $E_{Sn/Sn^2} = -394mV_{SSE}$. However, the content of Sn increases very rapidly with increas-

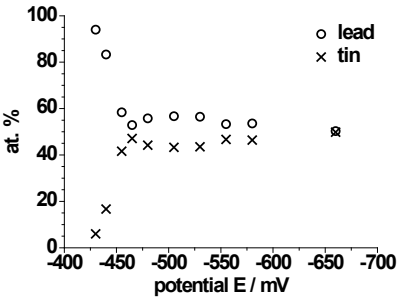

Fig. 8: Chemical composition determined by EDX-measurements

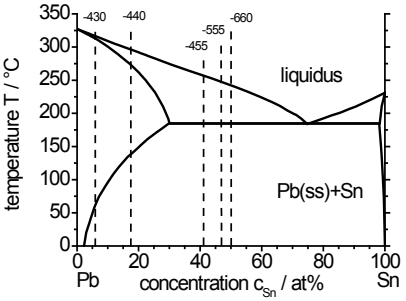

Fig. 9: Equilibrium phase diagram of Pb and Sn according to [19]. The broken line represent the theoretical phases of the electrolytic PbSn layers depending on the deposition potential and the EDX-analysis (based on the results of Figs.4 and 7)

ing overvoltage according to the increasing influence of the mass transport at the electrode kinetic. Within a potential range according to region II (diffusion controlled region) in *Figure 4* the relation between Pb and Sn is nearly constant. Thereby, the content of Pb in the layers is approximately between 5% and 10% higher than the content of Sn, although the bulk concentration of both ions in the electrolyte is the same. This difference could be explained by the differences in the diffusion coefficients of the ions in the electrolyte. Otherwise, the only measurement value of a sample from region III – where the deposition kinetic is also controlled by the diffusion – shows a relation between Pb and Sn of 1. However, the accuracy of the EDX-measurement of this sample could be influenced by the distinct appearance of dendrites. If we assign the layer composition based on the EDX-measurements (*Fig. 8*) to the equilibrium phase diagram (*Fig. 9*) we can expect a two-phase microstructure consisting of a Pb-solid solution and pure Sn at any deposition potential. Only the layer deposited at E=–430mV and room temperature can be described as a single-phase layer, according to the equilibrium phase diagram, because the Pb-solid solution can consist of up to 95at.% of Pb and 5at.% Sn at 293K (20°C) [21].

It is evident that the variation of the deposition potential allows a wide variation of the chemical composition of Pb-Sn layers approximately between PbSn95-6 and PbSn50-50. According to the chemical composition the phase constitution should also vary quantitatively between a lead rich alloy which mainly consists of a Pb solid solution and a small amount of β-Sn and a dual phase alloy with a phase relation of approximately 1:1. At the highest applied potential the composition of the alloy corresponds with the electrolyte composition that was used. Consequently, the weight of the PbSn layer decreases with an increasing content of Sn as measured on the spot tests (*Tab. 2*).

X-ray analysis

Three different PbSn layers (deposited at E=–430mV, E=–455 and E=–555mV) have been investigated by x-ray diffraction. *Figure 10* shows the xrd-pattern. All diffractograms show Bragg-reflexes of the Au-substrate. The information depth of the x-ray diffractometry is in the range of 5µm to 7µm, whereby the thickness of the PbSn-layers amounts to approximately 2µm. According to the results of the EDX-analysis (*Fig. 8*) the diffractogram of the layer deposited at E=–430mV shows only the strongest Sn-reflex (200) beside the reflexes of Pb. The diffractograms of layers deposited at E=–455mV and E=–555mV shows the complete pattern of Sn because the Sn content of the layer clearly increases at higher overvoltages. *Figure 10b* shows a section of a diffractogram of a PbSn-layer deposited at E=–430mV. Between the diffraction angle (2θ) of 40° and 42° two weak Bragg reflexes appear, which correspond with a AuSn-layer. Unfortunately, these

Tab. 2: Gravimetric spot tests of PbSn layer (the deposited charge is always the same)

Deposition potential / mV_{SSE}	–450	–500	–525	–550
Weigth layer / µg	942	916	913	913
Layer thickness / µm	1,95	1,91	1,9	1,93
Current efficiency	0,97	0,99	0,99	0,97

reflexes are not detected in all the measured layers deposited at E=–430mV. Nevertheless, the existence of such a very thin AuSn is understandable according to the cyclovoltammogram shown in *Figure 1b and 2*, where a small peak hints at an under potential deposition of Sn on the gold substrate. A thin layer of AuSn can be formed as start layer. A similar phenomenon is reported by R. J. Nichols et al. [25] and T. Will [26]. In the case of an over potential deposition of copper on gold,

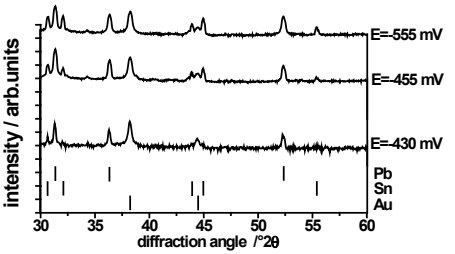

Fig. 10a: X-ray diffraction pattern of PbSn-layer deposited at E=–430 mV, E=–455 mV and E=–555 mV

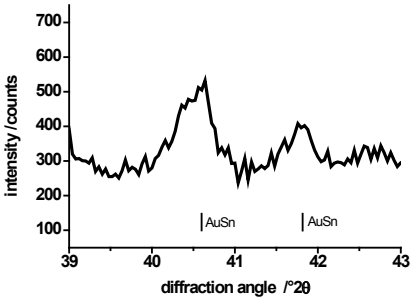

Fig. 10b: Section of diffractogram between 2θ=39° and 2θ=43° (E=–430mV)

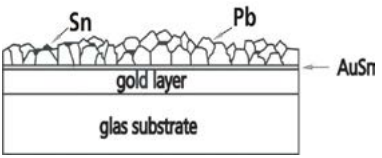

Fig. 11 Scheme of the microstructure of a PbSn-layer formed on Au in a sulphonate based electrolyte in the range (I)

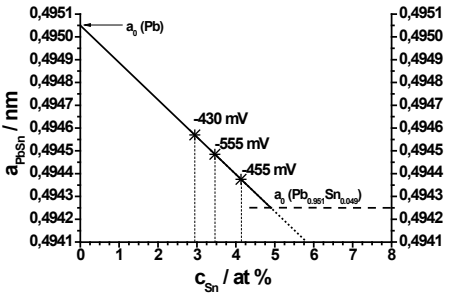

Fig. 12: Lattice parameter of Pb solid solution versus Sn content. The broken line represents the maximum of the displacement at the maximum content of Sn according to [19]

Tab. 3: Lattice parameter, parameter displacement and calculated concentration of Sn in Pb solid solution

E / mV	a_{PbSn} / nm	Δa / nm	c_{Sn} / at.%
–430	0.49457 ±0.00001	0.00048 ±0.00002	2.9
–455	0.49437 ±0.00001	0.00068 ±0.00002	4.1
–555	0.49448 ±0.00001	0.00057 ±0.00002	3.5

they observed an electrochemical alloy between copper and gold. *Figure 11* schematically shows the microstructure of PbSn-layer formed by electrolytic deposition from a sulfonat based electrolyte. On a very thin layer of AuSn the Pb and the Sn phase grow separately and the layer formation is compliant with the *Stranski-Krastanov* growth mode [27].

Additionally, the authors evaluated the measured lattice parameter of Pb. According to *Vegard's* rule we would expect that the lattice parameter a_{Pb} would decrease with an increasing Sn content in the Pb solid solution [29]. The theoretic lattice parameter of pure lead is a_0=0.49505nm [13]. The theoretic lattice parameter of the Pb solid solution with thermodynamic maximal Sn content (4.9at%) is a_{Pb}=0.49425nm [19, 21]. Tyzack et al. [21] and recently Bondarenko et al. [28] reported that the displacement of the lattice parameter in the Pb solid solution up to a content c=4.9at% Sn does not significantly deviate from a straight line.

This allows for a graphic estimation of the Sn content which is solved in the Pb solid solution at various deposition potentials (*see also Tab. 3*). The measured parameter a_{Pb} plotted on the solid line (*Fig. 12*) and the intersection of the perpendicular line with the x-axis results in the Sn content in the Pb solid solution.

The results shown that less than the maximum (4.9at%) of Sn is solved in the Pb solid solution. Otherwise, the overall content of Sn in the deposited PbSn layer is never less than 6at% (*see Fig. 8*). That means that the formation of β-Sn as a separate phase proceeds independently of the chemical composition of the Pb solid solution. The incorporation of Sn in the Pb solid solution does not correlate with the deposition potential. A supersaturated Pb solid solution as reported for electrolytic deposition of NiAg [24] is not found.

4 Summary

The present work focuses on the formation and microstructure of electrochemically deposited Pb-Sn-layer.

According to the cv measurements a upd of Sn onto the gold substrate is assumed as the initial process. This can be associated with an electrochemical alloy and the formation of a very thin AuSn intermetallic phase. Subsequently, the layer formation is determined by the co-deposition of a Pb solid solution and β-Sn. Consequently, the layer formation follows the *Stranski-Krastanov* mechanism. The work has shown that both phases form a layer with a dual phase microstructure. Thereby the content of Sn in the complete layer is strongly dependant on the deposition potential and could amount up to 50 at% in maximum. In contrast, the Sn content solved in the Pb solid solution does not correlate to the deposition potential. The formation of a non-equilibrium alloy consisting of supersaturated Pb solid solution was not observed. Depending on the overvoltage the kinetic of the layer formation can be divided in an active or mixed controlled range (I) a diffusion controlled range (II) and a diffusion controlled range with extreme surface enlargement (III). The morphology varies from being cauliflower-like to spongy. There is no hint of a clear correlation between the grain size and the deposition potential, respectively, the deposition current density. Side reactions such as hydrogen evolution are not observable. This is in a good agreement with the theory of the high over voltage for the hydrogen reduction on Pb as well as Sn. Therefore the current efficiency is close to 100%.

Acknowledgment

The authors would like thank gratefully the German Research Foundation (DFG) for the financial support under grant SCHN745/4-2.

Literatur

[1] G. Strube, Galvanotechnik 73 (1982)1330

[2] B. Gaida, K. Aßmann, Rechnologie der Galvanotechnik, Eugen G. Leuze Verlag, Saulgau /Württ. 1996, pp.274–283

[3] M. Merkel, K.-H.Thomas, Technische Stoffe Fachbuchverlag Leipzig, pp.266–272t

[4] A. Brenner, Electrodeposition of Alloys, Vol.1, Academic Press, New York, 1963

[5] J.L. P.Siqueira, I.A. Carlos, J. Power Sorces 169 (2007) 361

[6] G. Schulze: Die Metallurgie des Schweißens, Springer Verlag Berlin Heidelberg, 2004

[7] M. Merkel, K-H. Thomas: Taschenbuch der Werkstoffe, Fachbuchverlag Leipzig im Carl Hanser Verlag, Leipzig, 2008

[8] H.Schumann, H. Oettel: Metallografie, WILEY-VCH, Weinheim, 2005

[9] H. Fischer, Elektrolytische Abscheidung und Elektrokristallisation von Metallen, Springer Verlag Berlin 1954, p.729

[10] F. Palmisano, E. DesimoniL. Sabbatini, G. Torsi, J. Appl. Electrochem. 9 (1979) 517

[11] I. Petersson, E. Ahlberg, J. Electroanal. Chem. 485 (2000) 166

[12] I. Petersson, E. Ahlberg, J. Electroanal. Chem. 485 (2000) 178

[13] D. R. Lide, CRC Handbook of Chemistry and Physics, CRC Press, Boca Raton, 1992

[14] V.A. Vicente, S. Bruckenstein, Anal. Chem. 44 (1972) 297

[15] M. Paunovic, M. Schlesinger: „Fundamentals of Electrochemical Deposition" J. Wiley & Sons, Inc. New York u.a.O. 1998 pp.90ff

[16] H. Fischer: Zeitschrift Elektrochemie 54 (1950) 459

[17] R. Winand, Electrochimica Acta 39 (1994) 1091

[18] D. Landolt, Electrochimica Acta 39 8/9 (1994) 1075–1090

[19] ASM Alloy Phase Diagrams Center, P. Villars, editor-in-chief; H. Okamoto and K. Cenzual, section editors; http://www.asminternational.org/AsmEnterprise/APD, ASM International, Materials Park, OH, USA, 2006, 2007, 2008, 2009, 2010

[20] J.W.Dini cit. in I. Handreg: Dissertation Bergakademie Freiberg, Freiberger Forschungsheft B285, 1998 S.5

[21] C. Tyzack, G.V. Raynor, Acta Crystallogr., 7 (1954) 505

[22] V. Danel, V.Plichon, Electrochimica Acta 27 (1982) 771

[23] J. Torrent-Burgués, E. Guaus, Portugalia Electrochimica Acta 23 (2005) 471

[24] M. Schneider, A. Krause, M. Ruhnow, J. Mat. Sci. Letters 21 (2002) 292

[25] R.J. Nichols, D.M. Kolb, R.J. Behm, J. Electroanal. Chem. 313 (1991) 109

[26] T. Will, „Untersuchung zur Kupferabscheidung auf Au(111)-Elektroden: eine in-situ STM Studie" dissertation thesis Universität Ulm 1994,p.98

[27] E. Budevski, G. Staikov, W.J. Lorenz, "Electrochemical Phase Formation and Growth" VCH-Verlagsgesellschaft mbH, Weinheim 1996, p.5

[28] Y.O. Bondarenko, N.F. Voronina, O.A. Shmatko, Defect and Diffusion Forum, 277 (2008) 193

[29] L. Vegard, Zeitschrift für Physik A Hadrons and Nuclei Volume 5, Number 1 (1921), 17–26, DOI: 10.1007/BF01349680

[30]E. Gomez, E.Guaus, F. Sanz, E. Valles, J. Electroanal. Chem. 465 (1999) 63

Corresponding author:

Dr.-Ing. M. Schneider
Fraunhofer Institute for Ceramic Technologies and Systems Dresden, Winterbergstr. 27, 01277 Dresden, Germany

Author:

Dipl.-Ing. K. Kremmer
Fraunhofer Institute for Ceramic Technologies and Systems Dresden, Winterbergstr. 27, 01277 Dresden, Germany

Author:

Dipl.-Ing. B. Matthey
Fraunhofer Institute for Ceramic Technologies and Systems Dresden, Winterbergstr. 27, 01277 Dresden, Germany

CONTACT:

EUGEN G. LEUZE VERLAG KG
Ralf Schattmaier
Karlstraße 4
88348 Bad Saulgau
Germany

Email: ralf.schattmaier@ecv.de
Phone: ++49(0)7581-4801-12
Fax: ++49(0)7581-4801-10